TECHNICAL ARTICLE

Evaluation of a Processing Route and Microstructural Characteristics for the Development of Ultrafine Bainite in Low-Temperature Ausformed Medium-Carbon Steels

Pentti Kaikkonen [ID], Mahesh C. Somani, Aarne Pohjonen, Vahid Javaheri, and Jukka Kömi

A combination of physical simulation and laboratory rolling experiments, including thermomechanical rolling and low-temperature ausforming, was conducted for designing a suitable processing route to enable phase transformation from austenite to ultrafine bainite in a medium-carbon steel. Following low-temperature ausforming at 500-550 °C, two different cooling and holding paths were tried in the study: (1) water cooling close to martensite start temperature (300 °C), followed by isothermal holding (route A), and (2) air cooling to 350 °C followed by isothermal holding (route B). For reference, a third sample was directly water-cooled to 300 °C after hot rolling without ausforming treatment, followed by isothermal holding (route C). Field emission scanning electron microscopy and electron backscatter diffraction, as well as x-ray diffraction, were employed for microstructural analysis and correlations with the mechanical properties evaluated in respect of hardness and tensile properties. The low-temperature ausforming and subsequent cooling schedules resulted in the decomposition of austenite into ultrafine bainite and some martensite, while stabilizing a fraction of finely divided, carbon-enriched interlath austenite. Results suggested the development of a novel, multiphase bainite-martensite-austenite microstructure, achieved via low-temperature ausforming and subsequent air-cooling (route B), was beneficial in respect of mechanical properties. Most of the bainitic plates were in the range of 50-200 nm with the occasional presence of coalesced plates as wide as 2000 nm. Despite the differences in the microstructure, the mechanical behavior of non-ausformed samples was not significantly different. The technique paves way for developing medium-carbon nanostructured/ultrafine bainitic steels with high mechanical properties achieved via innovative modification of processing routes including low-temperature ausforming.

1. Introduction

The potential of a multiphase microstructure comprising essentially ultrafine bainitic ferrite (BF) with a small fraction of finely divided carbon-enriched austenite, in imparting ultrahigh strength (> 1500 MPa) combined with good tensile ductility, adequate low-temperature toughness, and high strain hardening capacity, has been well established. In the early 2000s, Caballero et al. (Ref 1) and Caballero and Bhadeshia (Ref 2) reported the formation of extremely fine (< 50 nm) bainite plates in high carbon steels, often referred to as nanostructured bainite, achieved through specific composition and process designs. A combination of ultrahigh tensile strength (1700-2200 MPa) originating from the fineness of BF plates, adequate

ductility (5-30%), and fracture toughness (30-50 MPa·m$^{1/2}$) imparted by the fine division of interlath retained austenite (RA) outperformed every bainitic steel developed thus far (Ref 3).

In recent years, frantic efforts have been made to shorten the isothermal holding durations to enable the occurrence of bainitic transformation in reasonable times essentially by reducing the carbon content in steels (Ref 4, 5). On the other hand, the reduction of carbon in the steel to a reasonable level can also improve the usability properties, such as weldability and bendability, while enabling the accomplishment of an excellent combination of mechanical properties at par with high carbon nanostructured bainitic steels (Ref 1, 2). In this context, Hu et al. (Ref 6) reported that the ausforming of medium-C steels at 400 °C accelerated the kinetics of bainite formation during subsequent isothermal holding at 300 °C, compared to the samples ausformed at marginally higher temperatures (450 and 500 °C) that resulted in deceleration of transformation kinetics under similar conditions. However, according to Kaikkonen et al. (Ref 7), 0.4 wt.% C steels displayed a tendency for strain-induced accelerated transformation following ausforming at all temperatures below 500 °C, especially at 300 and 400 °C, but with a concomitant increase in flow stress and rolling loads. On the other hand, Zorgani et al. (Ref 8) concluded that ausforming above bainite start (B_s) temperature neither did affect the bainite plate thickness, nor its morphology, though the initial transformation rate was slightly enhanced, with the overall bainite fraction somewhat decreased

Pentti Kaikkonen, Mahesh C. Somani, Aarne Pohjonen, Vahid Javaheri, and **Jukka Kömi**, Materials and Mechanical Engineering, Centre for Advanced Steels Research, University of Oulu (Oulun yliopisto), 90014 Oulu, Finland. Contact e-mails: pentti.kaikkonen@oulu.fi, mahesh.somani@oulu.fi, aarne.pohjonen@oulu.fi, vahid.javaheri@oulu.fi, and jukka.komi@oulu.fi.

Graphical Abstract

P. Kaikkonen, M. Somani, A. Pohjonen, V. Javaheri, J. Kömi
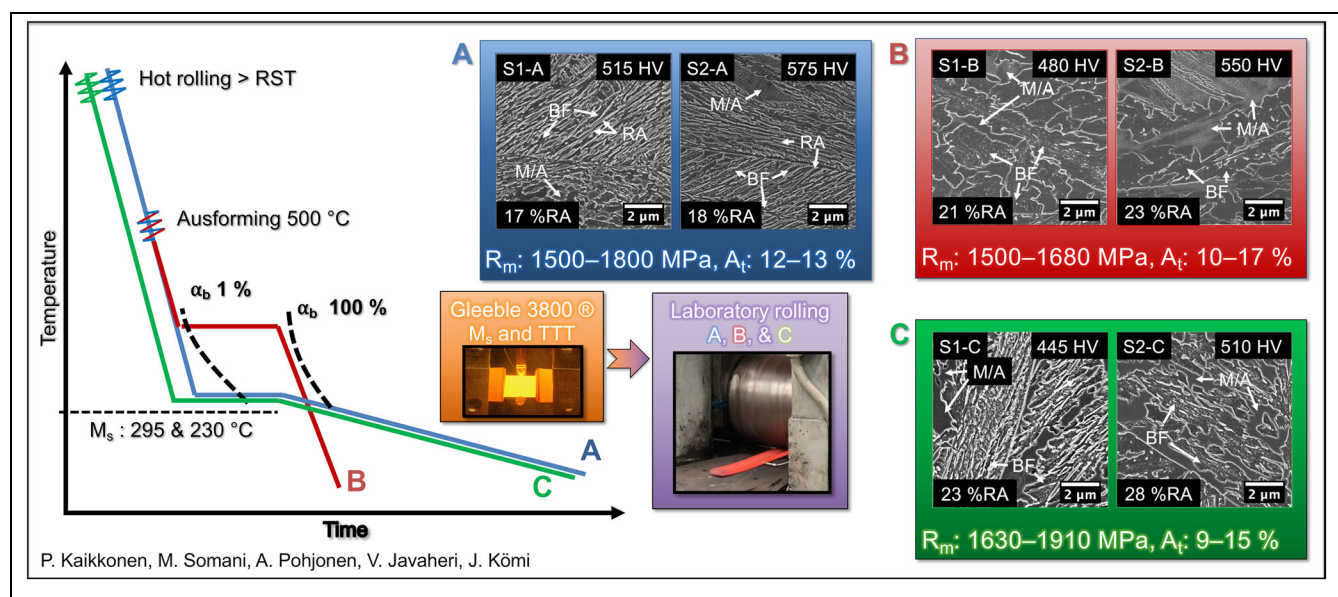
in comparison with the samples processed without prior ausforming.

The contribution of nanostructured bainite to the magnitude of strength depends mainly on its BF plate thickness, whereas the ductility is controlled by the RA fraction, fineness, and its stability, basically through the transformation induced plasticity (TRIP) effect (Ref 9). Zhang et al. (Ref 10) reported the formation of nanostructured bainitic laths finer than 100 nm in medium-C steels, following optimized ausforming in the range of 300-600 °C and subsequent isothermal bainitizing conducted in a narrow range of 235-250 °C, thus resulting in high hardness (600-650 HV). Zorgani et al. (Ref 11) reported the presence of blocky RA in samples subjected to ausforming at 600 °C, followed by isothermal bainitic transformation above 350 °C, whereas samples bainitized at a marginally lower temperature (325 °C) resulted in very stable RA regardless of the ausforming strain. Li et al. (Ref 12) applied two-step isothermal holding in order to obtain a higher fraction of fine, film-like retained austenite besides the refined grain size of blocky retained austenite, resulting in improved tensile properties compared to the results of one-step isothermal holding.

A few controversies concerning the influence of low-temperature ausforming on the microstructures of bainitic steels have been pointed out in the literature as well, though some of them depend on the ausforming conditions. Eres-Castellanos et al. (Ref 13) reported that due to the anisotropy caused by low-temperature ausforming prior to isothermal holding, it might not be possible to appropriately measure the bainite plate thickness without actual 3D observation of the microstructure, as the plates tended to tilt toward the direction perpendicular to the deformation axis. Besides, they compared the plate thicknesses of BF in different steels after conducting similar treatments including low-temperature ausforming and observed significant variations in plate thicknesses of the three studied steels (Ref 14). However, the same authors also reported that a decreased fraction of BF, obtained after low-temperature ausforming and isothermal holding, was not only because of mechanical stabilization of RA but also due to the tendency of

strain and/or stress-induced martensite formation at high stress levels, even above the M_s temperature (Ref 13-15). Similarly, it was explained by van Bohemen (Ref 16) that during the growth of bainite, the dislocation density of austenite might exceed the overall dislocation density due to mechanical stabilization, as a consequence of plastic deformation resulting from ausforming and elastic strains from the bainite growth itself. In contrast with the previous studies, Avishan et al. (Ref 17) reported that even a low ausforming strain of 10% at 300 °C did increase not only the fraction of nanostructured bainite but also enabled refinement of the bainite packets. Moreover, the enhanced mechanical stability of RA achieved by ausforming contributed to remarkably improved elongation of the nanostructured bainitic steels.

Hence, a good number of studies have explored the potential of ultrafine/nanostructured bainite and designing of optimal processing routes, while only a few studies are available in the literature that provide insights on the microstructural features and related mechanical properties corresponding to the practical laboratory-scale processing routes. These replicate the operations of industrial rolling mills, instead of ideal dilatometer-based approaches adopted on a thermomechanical simulator. This study aims at developing and evaluating processing route/s for achieving ultrafine (preferably < 100 nm) bainite with small fractions of finely divided RA in two medium-carbon steels. Suitable cooling paths, ausforming parameters, and isothermal holding times were sought by conducting physical simulation experiments in a Gleeble 3800® thermomechanical simulator, and accordingly, three different processing routes including one reference path without low-temperature ausforming were designed for laboratory rolling experiments and subsequent cooling of large samples in order to preliminarily evaluate the microstructures and mechanical properties. The influence of different processing routes comprising laboratory-scale rolling and subsequent cooling along different paths, with or without low-temperature ausforming, on the microstructures and mechanical properties is presented comprehensively in

order to improve the understanding of processing-microstructure-property relationships of medium-carbon bainitic steels.

2. Materials and Methods

2.1 Materials

The chemical compositions and experimentally estimated M_s and calculated B_s (Ref [18]) temperatures of two medium C steels S1 and S2 used in this study are shown in Table 1. The carbon contents of the experimental steels were varied at two levels, 0.4 wt.% C and 0.48 wt.% C for S1 and S2, respectively. A semi-empirical thermodynamic-kinetic software IDS® (Ref [19]) was used in finetuning of the alloy design to minimize the segregation of alloying elements during casting while maintaining adequate hardenability with suitable additions of 2.0 wt.% Mn and 0.7 wt.% Cr. In addition, a commercial software JMatPro® v8.0 was used to plot the continuous cooling transformation (CCT) diagrams to determine appropriate low-temperature ausforming conditions as well as a suitable range of bainitizing temperatures close to M_s temperature for subsequent isothermal holding. A high level of Si (1.3%) was added in both steels to hinder the precipitation and growth of carbides during isothermal holding. Both V and Nb were added for realizing an appreciable strengthening effect via precipitation strengthening, while Nb enabled the control of grain size in reheating and influenced grain refinement during hot rolling and subsequent refinement of BF with a concomitant improvement in toughness (Ref [20]).

2.2 Methods

The rough-rolled and homogenized (1250 °C for 24 h) blocks of dimensions $38 \times 50 \times 180$ mm were used for laboratory rolling experiments. One such 38 mm thick block of each composition was hot rolled down to a 12-mm-thick plate to enable the preparation of specimens of dimensions ø6 × 9 mm for conducting thermomechanical simulations using the Gleeble simulator. The physical simulation of the thermomechanical process (see Fig. 1a) consisted of three consecutive steps: 1) reheating (austenitization) at 1000 °C for 3 min, 2) low-temperature deformation of austenite (ausforming) at 500 °C, and 3) isothermal holding at different temperatures close to M_s temperature, followed by cooling to room temperature (RT). In the course of these three steps as well as after the final step, samples were cooled at an average linear cooling rate of 25 °C s^{-1}, which was also significantly higher than the critical cooling rate of ~ 2 °C·s^{-1} of S1 steel with 0.4 wt.% C (Table 1), as revealed by the CCT diagram plotted using JMatPro® software and also preliminary dilatation tests (Ref [21, 22]). The isothermal holding temperatures (T_{IH}) were chosen in narrow ranges of 300-400 and 275-375 °C, in steps of 25 °C, for steels S1 and S2, respectively.

The most appropriate isothermal holding conditions for bainite transformation were chosen based on the outcome of physical simulation experiments in terms of hardness values and phase fractions obtained. The ausforming temperature (500 °C) and strain (~ 0.30) were selected based on the literature information and the authors' previous research (Ref [7]). Ausforming was conducted just above the B_s temperature and below the ferrite/pearlite C-curves to prevent any strain-induced transformation during ausforming. Though the selected ausforming temperature (500 °C) was somewhat high, it was still chosen in order to be able to impose a nominal strain of ~ 0.3 in austenite with reasonable rolling loads available in accord with the capacity of the mill.

Three different processing routes A, B, and C employed in laboratory rolling simulations are illustrated schematically in Fig. 1(b). Initially, all the samples were reheated at 1250 °C for 90 min, followed by hot rolling in three consecutive passes of ~ 0.05, 0.22, and 0.26 true strains to the final thickness of ~ 19 mm, while the temperature dropped sharply to ~ 1050 °C. The samples were then subjected to water-cooling down to the ausforming temperature (500 °C). In the case of route A, the samples were further rolled (ausformed) to a final thickness of 12 mm in two consecutive passes, thus imparting a strain of ~ 0.3, followed by water cooling to T_{IH} at 300 °C on a run-out table at an average cooling rate of 20 °C s^{-1}. The water was sprayed through four nozzles; two of them were located above the run-out table and the other two below it. In the case of route B, the hot-rolled samples were ausformed at 500 °C similarly as in the case of route A, but these were subsequently air-cooled to T_{IH} at 350 °C at an average cooling rate of 0.5 °C s^{-1}. Route C was included as a reference path, wherein the hot-rolled samples were water-cooled at an average cooling rate of 20 °C s^{-1} directly to T_{IH} at 300 °C, without conducting the ausforming treatment at 500 °C.

In the case of routes A and C, following isothermal holding (60 and 90 min for steels S1 and S2, respectively), the furnace was switched off and the samples were allowed to cool slowly in the furnace down to RT at an average cooling rate of 0.01 °C s^{-1}. On the other hand, in the case of route B, the samples were taken out of the furnace after isothermal holding and immediately covered all around with 25 mm thick isolating alumina wool for controlled cooling down to RT at a slightly higher average rate of 0.1 °C s^{-1}.

The cross-sectional surfaces of the specimens (longitudinal in the case of rolled materials) were prepared for structural examination via the standard metallographic procedure, followed by etching with 2% Nital solution. Microstructures were observed in a Zeiss Sigma field emission scanning electron microscope (FESEM) operated at an accelerating voltage of 5 kV with an InLens detector. Selected specimens were suitably polished with colloidal silica (0.04 μm) solution for conducting electron backscatter diffraction (EBSD) measurements. EBSD scans were conducted at an accelerating voltage of 15 kV with an aperture size of 120 μm and a step size of 0.5 μm was used, while the scanned area was approximately 440 × 440 μm. Post-processing of the EBSD data was done using EDAX OIM (version 7) analysis software. Grains were defined based on a minimum misorientation angle of 3°, and the minimum size of four pixels constituted a grain. X-Ray diffraction (XRD) measurements were employed for estimating the RA fractions in all the specimens, using a Rigaku Smartlab x-ray diffractometer, operated with a Co-K α source at a scanning rate of 7° min^{-1} over the 2θ range of 45-130°. To determine the fractions of BF and martensite, the grid point counting method was used on multiple micrographs in accord with ASTM E 562 standard (Ref [23]). The average carbon concentration of RA (C_{RA}) was determined by substituting the value of lattice parameter a, calculated from the XRD measurements in Eq 1 (Ref [24]):

$$C_{RA} = (a - 0.3570\text{nm})/(3.8 \times 10^{-3}) \qquad (\text{Eq 1})$$

Table 1 Chemical compositions of the steels (in wt.%, Fe balance)

Steel code	C	Si	Cr	Mn	V	Nb	M_s, °C	B_s, °C*
S1	0.40	1.3	0.7	2.0	0.10	0.018	295	485
S2	0.48	1.3	0.7	2.0	0.10	0.021	230	468

*Calculated using the equation suggested by van Bohemen (Ref 18).
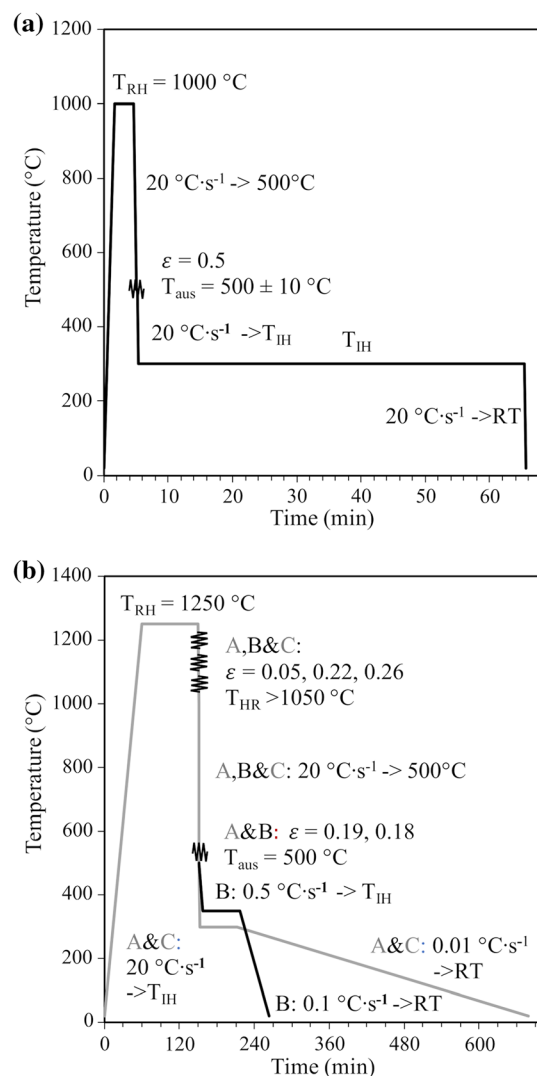
Fig. 1 A schematic diagram of (a) physical simulation testing in the Gleeble simulator and (b) thermomechanical processing routes a, b, and c employed in laboratory rolling. Holding times at T_{IH} (route a: 300 °C, routes b and c: 350 °C) were 60 and 90 min for steels S1 and S2, respectively. (Abbreviations: T_{IH} = isothermal holding temperature; T_{RH} = reheating temperature; T_{HR} = temperature of hot rolling; T_{aus} = temperature of ausforming)

Vickers hardness measurements were conducted on all the specimens using a test load of 10 kg (5 kg for physical simulation samples). Tensile tests were carried out on round specimens of the gauge dimensions Ø6 × 40 mm parallel length, prepared according to ASTM E 8 standard (Ref 25), and

tested at RT in a 100-kN Zwick Roell tensile testing device. The tensile properties were determined as an average of at least three test results for each condition.

3. Results

3.1 Microstructures of the Physical Simulation Specimens

Typical microstructures of steels S1 and S2 following physical simulation testing in the Gleeble simulator comprising isothermal holding at 350 and 375 °C are shown in Fig. 2. The corresponding hardness values and estimated RA fractions are included in Table 2. Hereinafter, the samples will be identified with the steel code and the numerical value of the corresponding T_{IH}, for instance, "S1-350" implies steel S1 after isothermal holding at 350 °C. While the RA phase fractions were estimated using the XRD data, the fractions of BF and martensite were assessed based on grid point counting on FESEM micrographs. The details of the phase fractions, plate thicknesses of BF (t_{BF}) as well as average C_{RA} are listed in Table 2. The microstructure of S1-350 (Fig. 2a) essentially comprised BF (71%) and RA (29%). However, the RA morphology similar to martensite/austenite (M/A) constituents also existed (such as the arrow pointing to 'RA' grain in Fig. 2(a)), though the possible formation of small fractions of martensite during final cooling could not be discerned from the dilatation tests as well as metallography, even at high magnifications. It should, however, be emphasized that the M/A constituents in the current study should not be confused with M/A islands which are often discussed in the context of welding metallurgy. A significant fraction of austenite in the matrix that undergoes carbon enrichment during bainitic transformation can be stabilized near the interfaces during final cooling, while the interior regions devoid of adequate carbon enrichment may transform into martensite (Ref 11). Also, the average bainite plate thickness was of no specific relevance, as the typical thickness varied in a wide range from 200 nm to as high as 1000 nm. Only a small bainitic region was marked by fine plate-like morphology, whereas a significant fraction of bainite was either granular type or consisted of coalesced plates.

S1-375, however, showed only about 40% BF, and the morphology was practically almost granular (Fig. 2c). Unlike in the case of S1-350 (Fig. 2a), martensite (33%) in S1-375 sample was predominantly present in the form of M/A grains, while BF (40%) comprised of coarse (500-2000 nm) granular islands embedded in the M/A matrix. Despite the same level of RA achieved in S1-350 (29%) and S1-375 (27%) samples, the S1-375 had a remarkably high amount of fresh (untempered, high-carbon) martensite (33%), transformed from carbon-enriched austenite during the final cooling from 375 °C to
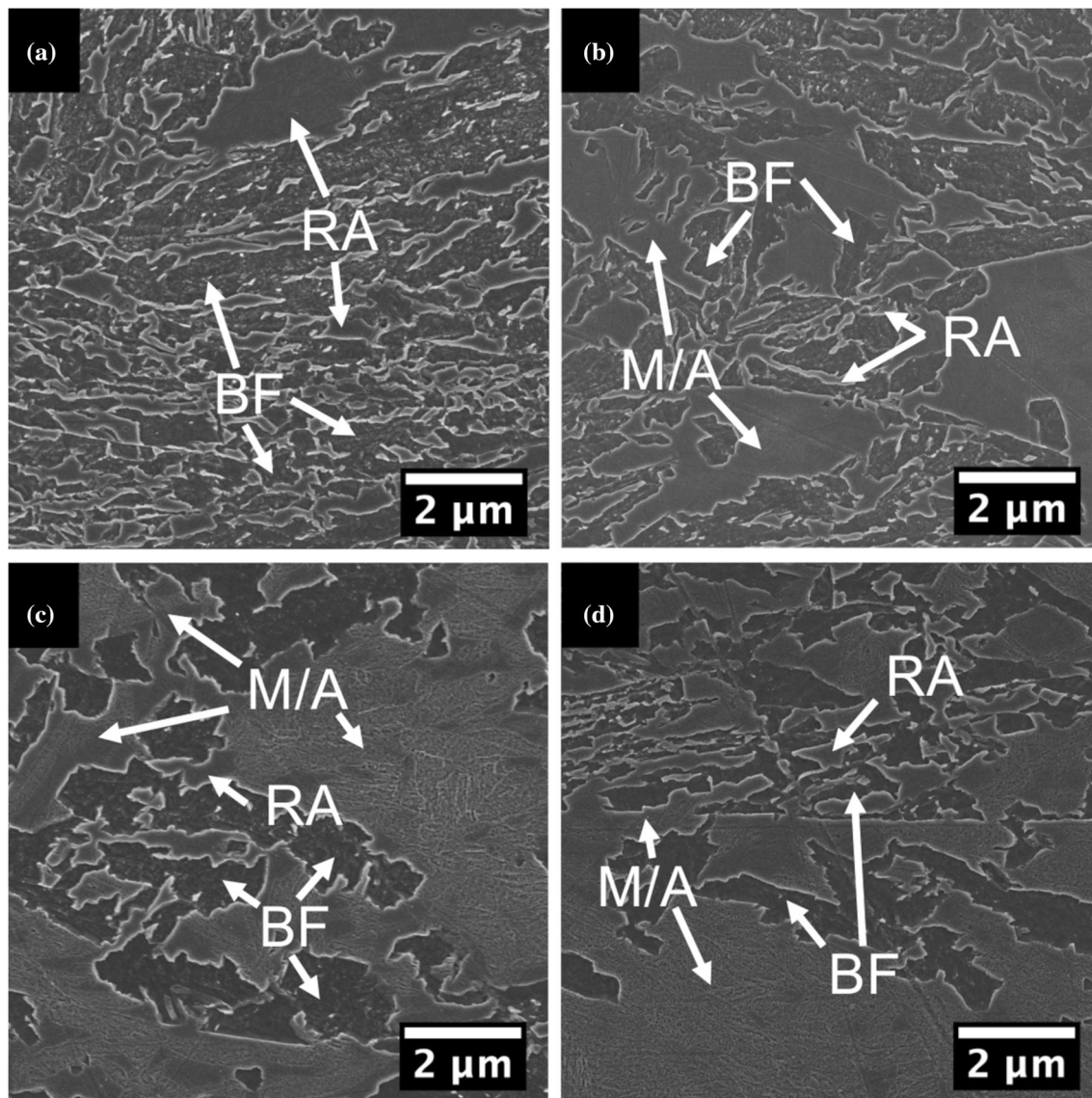
Fig. 2 Microstructures of steel S1 following physical simulation testing (Fig. 1a) and isothermal holding: (a) S1-350, and (c) S1-375. Similarly, for steel S2: (b) S2-350, and (d) S2-375

Table 2 Estimated phase fractions, bainitic ferrite plate thickness range (t_{BF}), and C_{RA} of Gleeble specimens following physical simulation tests. Corresponding hardness data are also included

ID	BF,%	M,%	RA,%	t_{BF}, nm	C_{RA} ,%	Hardness, HV
S1-350	71	0	29	200-1000	0.97	419
S1-375	40	33	27	500-2000	0.79	421
S2-350	42	24	34	300-1500	1.05	420
S2-375	22	60	18	300-1500	0.49	515

RT, unlike observed in the case of S1-350. All the same, Vickers hardness (421 vs. 419 HV) was practically at the same level, suggesting that at least some fraction of BF realized in S1-350 was significantly refined and the corresponding RA content adjacent to the BF ought to be more stable, owing to a high level of carbon partitioned from BF to relatively fine RA constituents (0.97 wt.% C_{RA}). On the other hand, isothermal holding at 375 °C resulted in a lower fraction of BF in the microstructure as well as lower carbon enrichment of the untransformed austenite (before final cooling to RT) and subsequent cooling resulted in a significant fresh martensite formation with slightly lower C_{RA} (0.79 wt.%).

In the case of steel S2, the microstructure of S2-350 (Fig. 2b) possessed a similar level of hardness (420 HV) as in the case of both S1 samples (S1-350 and S1-375; see Table 2) and the microstructural characteristics too comprised 34% RA,

42% BF (thickness range 300-1500 nm), and 24% high-carbon martensite present in large M/A constituents and were comparable to that seen in the case of S1-375. Even though the BF fraction was practically similar compared to the S1-375 (42 vs. 40%), RA fraction was slightly greater (34% vs. 27%) indicating that the higher carbon content in S2-350 could facilitate stabilization of more untransformed austenite with similar bainite content. Despite the lesser martensite fraction (24% vs. 33%), the corresponding hardness (419 HV), however, was at a level similar to those of S1-375 (421 HV) and S2-350 (420 HV), which was presumably a consequence of the higher carbon content of steel S2 (0.48 wt.%) compared to that of steel S1 (0.4 wt.% C). Besides, the C_{RA} in S2-350 was higher than that of S1-375 (1.05% vs. 0.79 wt.% C), which also explained the similar hardness levels of the two specimens despite the presence of a higher RA fraction and lower martensite content in S1-375. On the other hand, S2-375 (Fig. 2d) displayed only $\sim$ 22% bainite and retained about 18% austenite at RT, though with low C_{RA} (0.49 wt-% C) close to the nominal carbon content of the steel S2 (0.48 wt-% C). However, a large fraction of fresh martensite (60%) that formed during final cooling caused a significant increase in hardness (515 HV), which was about 23% higher than other samples.

3.2 Microstructures of Laboratory Rolled Specimens

Typical microstructures of steels S1 and S2, recorded in laboratory rolled and processed conditions, i.e., subsequent to the three routes A, B, and C (see Fig. 1b) comprising respective cooling paths and holding, are shown in Fig. 3. Corresponding phase fractions, t_{BF}, RA fractions, C_{RA} values, and hardness data are presented in Table 3. Hereinafter, the samples will be identified with the steel code and the corresponding processing route, for instance, "S1-A" means steel S1 processed through route A. The C_{RA} levels were estimated by substituting the lattice parameter data obtained from the XRD measurements in Eq 1. The microstructures of S1-A and S2-A (Fig. 3a and b) mostly consisted of fine BF (74 and 77% for S1-A and S2-A, respectively) with typical plate thickness in a narrow range of 50-200 nm, besides interlath RA films (15% each for S1-A and S2-A) of nearly similar thickness in between the bainitic plates. It should be emphasized that in spite of relatively higher carbon content (0.48 wt.%) in S2 steel, its bainite fraction was higher, presumably due to 50% longer isothermal holding time for bainitizing (90 min) compared to that of steel S1 (60 min). A longer holding time for steel S2 was justified, as an increased carbon content is known to delay the start of bainite formation as well as its kinetics. A small fraction of M/A constituents comprising fresh martensite formed during final cooling and blocky RA was observed in both S1-A and S2-A as well.

In contrast, the microstructures of S1-B and S2-B Fig. 3(c) and (d) displayed a remarkably high fraction of fresh martensite (20 and 25%, respectively), together with 59 and 52% of BF, respectively, whereas the corresponding RA fractions were of the nearly same level (21 and 23%, respectively). The morphology of BF looked more like coalesced bainite, as the films of RA adjacent to plates were almost completely missing, and the individual plates could not be detected in the FESEM study. It should be emphasized that the T_{IH} was different for routes A and B and may have significantly affected the morphology of BF and phase constituent fractions, similarly as in the case of Gleeble samples bainitized at T_{IH} of 350 and 375 °C (Fig. 2). Also, the slower final cooling rate in route B compared to route A may have influenced the BF plate morphology.

The microstructures of samples S1-C and S2-C processed through route C (Fig. 3e and f, respectively) seemed more like a mixture of structures seen in routes A and B. In effect, significant amounts of ultrafine ferritic bainite (67% and 60% for S1-C and S2-C, respectively) were present in the microstructures of both samples with the plate thickness varying typically in the range of 100-400 nm, even though the coarse granular and/or coalesced plate-like bainite (500-1000 nm) existed, too. While high fractions of austenite (S1-C: 23 and S2-C: 28%) were retained at RT both in the form of fine films (especially in S1-C) and blocky constituents, small fractions of martensite (S1-C: 10 and S2-C: 12%) were also observed in both the samples.

There was a systematic trend seen in respect of average hardness measured on the S1 and S2 samples for the three processing routes (see Table 3). Routes A and C imparted the highest and the lowest hardness, respectively, for both steel types, whereas route B resulted in a hardness intermediate between the two. Relatively higher hardness values of S2 samples compared to S1 samples regardless of the processing route can be attributed to the higher C content (0.48 wt.% C) of steel S2. Referring to Table 3, a quick comparison between routes A and C suggests that the higher hardness of S1-A (515 HV) and S2-A (575 HV) samples compared to those of S1-C (445 HV) and S2-C (510 HV) samples, respectively, can be attributed to a higher fraction of fine bainite (S1-A: 74, S1-C: 67%) and somewhat smaller fraction of RA (S1-A: 17 S1-C: 23%). A similar trend was seen in steel S2 also, as the corresponding fractions of BF (S2-A: 77 and S2-C: 60%) and RA (S2-A: 18 and S2-C: 28%) varied in the same direction.

High-angle (HAGBs) and low-angle (LAGBs) grain boundaries observed in the EBSD measurements of S2-A and S2-B are plotted in Fig. 4(a) and (b), respectively. Similarly, equivalent circle diameters (ECDs) of BF were calculated from the EBSD data, where the ECD evaluation consisted of grains constrained by low angle grain boundaries (2° to < 15°), as the interest was only focused on laths and plates of BF and M, and the corresponding distributions are shown in Fig. 4(c) and (d). The mean ECD of the S2-B sample was about 25% greater than that of S2-A (S2-A: 2.0 vs. S2-B: 2.5 μm).

3.3 Mechanical Properties

Selected mechanical properties are shown in Table 4 and graphically plotted in Fig. 5. Interestingly, the ultimate tensile strengths (R_m) were highest for the processing route B for both steels S1 and S2 (S1-B: 1630 MPa and S2-B: 1910 MPa) steels, obviously as a consequence of high martensite fractions in the steel samples (S1-B: 20 and S2-B: 25%). For S1 steel, R_m was the same (1500 MPa) for S1-A and S1-C samples, even though RA content achieved in S1-C (23%) was somewhat higher than that of S1-A (17%) and correspondingly, Vickers hardness was lower for S1-C (445 HV) compared to that of sample S1-A (515 HV). The highest total elongation A_t (17.0%) for steel S1 was obtained in S1-C sample, whereas the ductility of S2 samples was relatively lower (S2-A: 11.7%; S2-C: 10%). The fraction of fresh martensite was lower in S1-C (10%) sample compared to that of sample S1-B (20%), and this was reflected in relatively lower yield and tensile strengths of sample S1-C ($R_{p0.2}$ 730 MPa; R_m 1500 MPa) compared to those of S1-B ($R_{p0.2}$ 760 MPa; R_m 1500 MPa) sample. On the
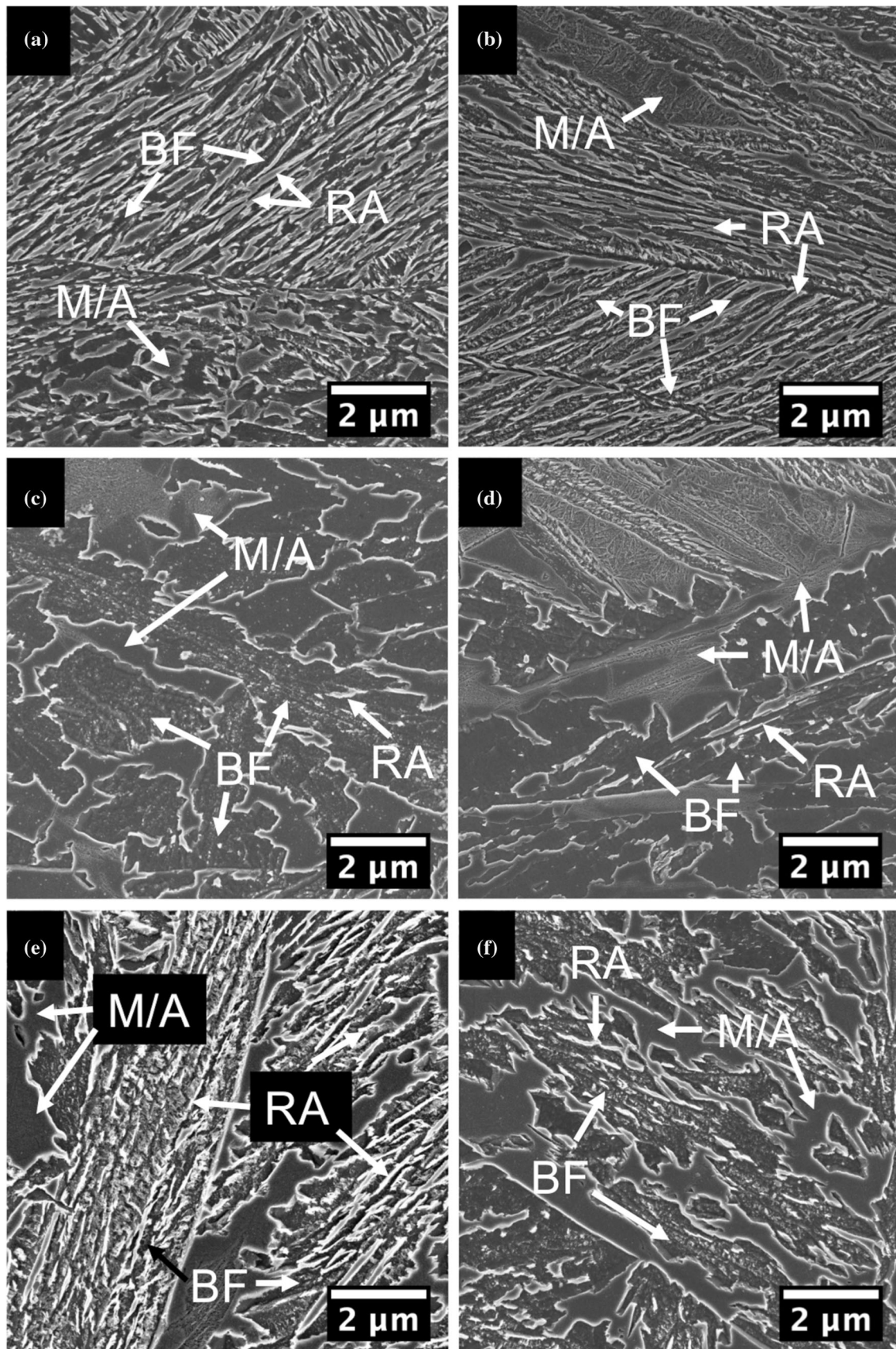
Fig. 3 Typical microstructures of steel S1 processed via different routes: (a) S1-a, (c) S1-b, and (e) S1-c. The corresponding microstructures of steel S2 are shown in (b) S2-A, (d) S2-B, and (f) S2-C, respectively

Table 3 Estimated phase fractions, bainitic ferrite plate thickness range t_{BF}, and C_{RA} of specimens following laboratory rolling and processing via routes A, B, and C. Corresponding hardness data are also included

ID	BF, %	M, %	RA_{total}, %	t_{BF}, nm	RA_{film}, %	RA_{block}, %	C_{RA}, %	Hardness, HV
S1-A	74	9	17	50-200	15	2	1.04	515
S1-B	59	20	21	500-2000	3	18	0.96	480
S1-C	67	10	23	100-1000	16	7	0.97	445
S2-A	77	5	18	50-200	15	3	1.02	575
S2-B	52	25	23	200-2000	1	22	1.01	550
S2-C	60	12	28	200-1000	11	17	1.18	510
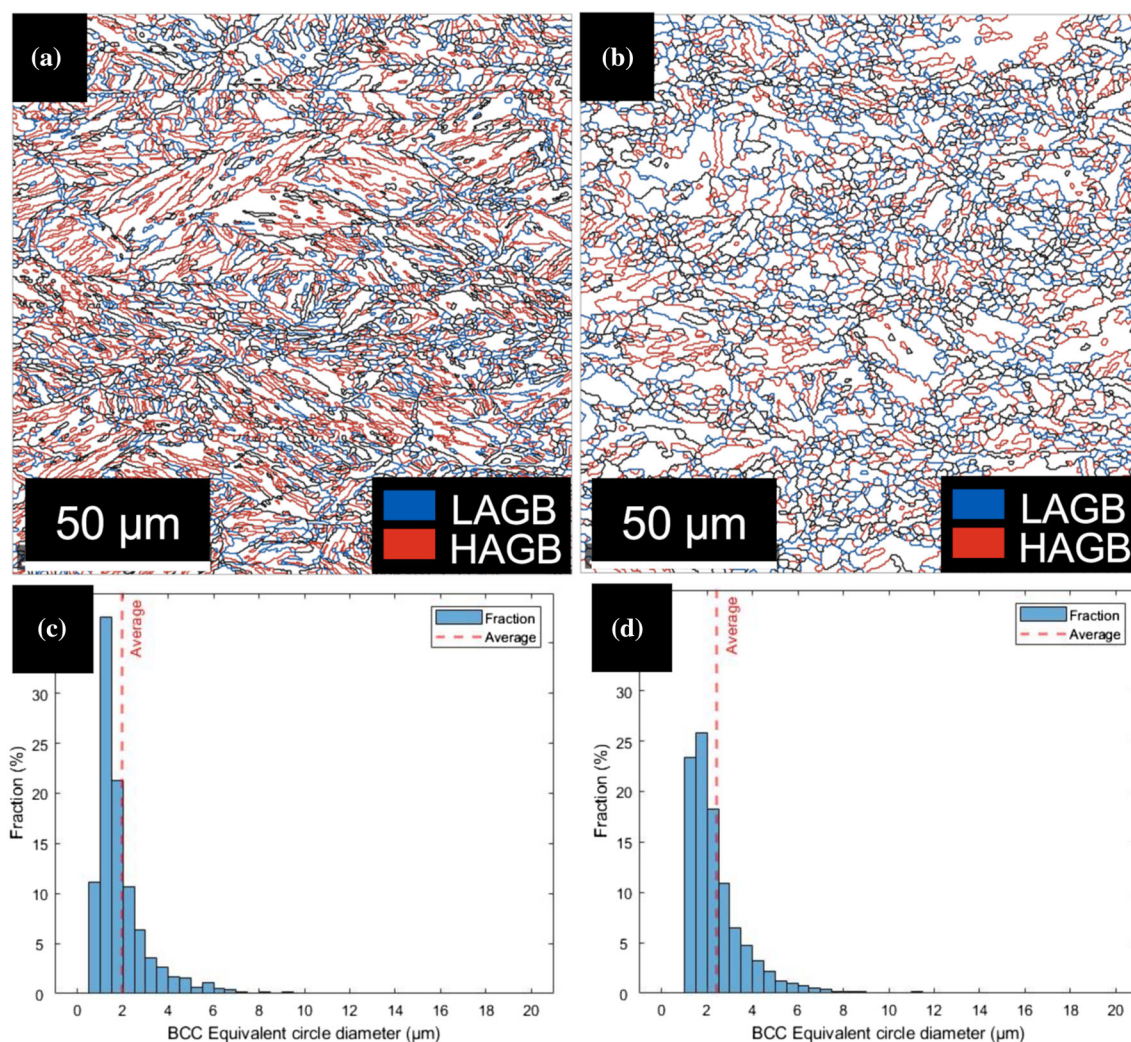
Fig. 4 High-angle (red) and low-angle (green) grain boundaries of (a) S2-a and (b) S2-b. Corresponding ECD distributions are presented in (c) and (d), respectively (Color figure online)

other hand, a high RA content in samples processed through route C (S1-C: 23%, and S2-C: 28%) expectedly contributed to ductility, though the differences were not as remarkable in the case of steel S2, as they were for steel S1. For steel S2, sample S2-A possessed the highest total elongation (A_t 11.7%) and $R_{p0.2}$ (960 MPa), though the corresponding R_m (1800 MPa) was only marginally lower than the highest value recorded for sample S2-B (1910 MPa), which is also illustrated in Fig. 5.

4. Discussion

4.1 Routes Efficiency

Routes A, B, and C were designed on the basis of physical simulation experiments, not only in terms of microstructural evolution but also considering the adoptability of the routes in industrial rolling environment, since the specimens of large

Table 4 A summary of tensile properties*, hardness, and RA contents obtained on the experimental steels processed through the three routes

ID	Processing route	$R_{p0.2}$, MPa	$R_{p1.0}$, MPa	R_m, MPa	A_g,%	A_t,%	Hardness, HV
S1	A	930 ± 16	1330 ± 6	1500 ± 2	5.4 ± 0.1	12.8 ± 0.1	515
	B	760 ± 15	1170 ± 10	1630 ± 18	11.3 ± 0.7	14.9 ± 0.6	480
	C	730 ± 19	1080 ± 14	1500 ± 17	11.9 ± 0.2	17.0 ± 0.1	445
S2	A	960 ± 18	1530 ± 5	1800 ± 4	5.5 ± 0.2	11.7 ± 0.2	575
	B	820 ± 6	1400 ± 4	1910 ± 5	7.9 ± 0.3	8.9 ± 0.3	550
	C	790 ± 11	1180 ± 15	1680 ± 15	9.0 ± 0.2	10.0 ± 0.2	510

*Average of three measurements, $\pm$ standard error, Rp0.2% and Rp1.0% are 0.2% and 1.0% proof strengths, respectively. R_m, A_g, and A_t stand for ultimate tensile strength, uniform elongation, and total elongation, respectively.
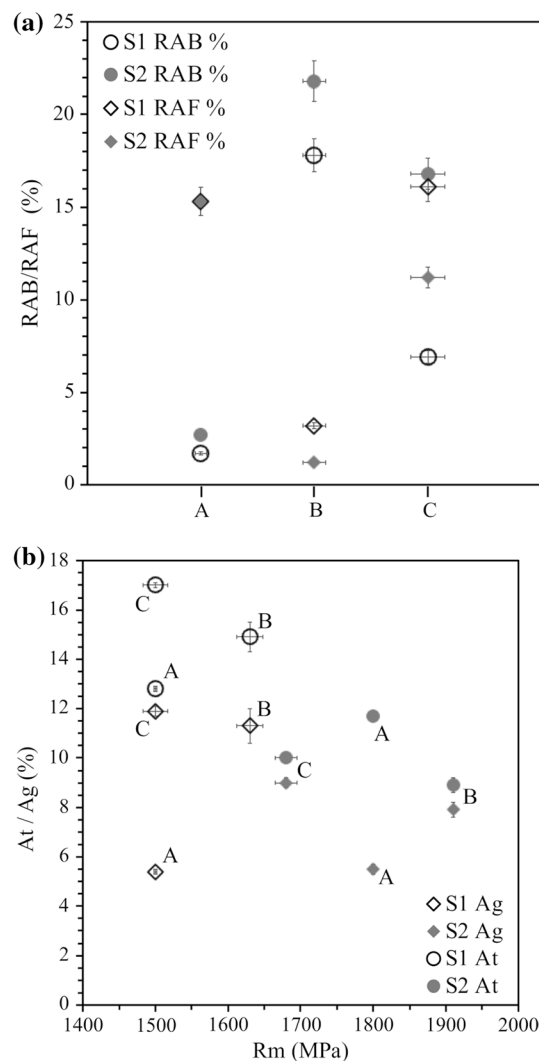

Fig. 5 (a) RA content (%) in the form of films (RAF) and blocks (RAB), plotted for the three processing routes a, b, and c, and (b) uniform elongation (A_g), total elongation (A_t) vs. the tensile strength (R_m) for the three processing routes a, b, and c

lation, since the calibrated water cooling line in route A allowed the realization of high cooling rates down to desired T_{IH}. This in turn prevented or at least minimized the formation of coarse upper bainite. As the temperature was measured and controlled in the mid-thickness of the rolled specimens, the temperature gradient through the thickness of the specimen was assumed to be steeper in the case of water-cooled samples (routes A and C), in comparison with the air-cooled specimens (route B). In our previous study (Ref 26), it has been noted that during the course of water cooling, the temperature on the surface might drop lower by even 50-70 °C than in the mid-thickness of the samples. Nevertheless, in route B, the T_{IH} was marginally higher (375 °C) compared to that of route A (350 °C) and was reached slowly via air-cooling resulting in two advantages: (1) enabled avoiding steep temperature gradients inside the sample as noticed in water-cooled samples and (2) permitted more accurate control of the temperature during cooling. Although water cooling was necessitated as a tool to achieve high cooling rates, it turned out to trigger sudden fluctuations in temperature leading to the possibility of small variation in uniformity of microstructure across the thickness. Route C, however, offered a simpler solution as the water cooling was applied all the way from the hot rolling stage to T_{IH} without the need for an ausforming step that entailed high load requirements and controlled deformation owing to the poor workability of austenite at these temperatures. Also, the process seemed beneficial in terms of the time gained to reach the lower bainite region, whereas in routes A and B, not only the intervening time from the ausforming step to the T_{IH} was short, but also the prior straining could trigger the start of strain-induced bainite transformation at temperatures higher than the desired T_{IH}. Moreover, as the isothermal holding time and subsequent cooling rate were kept similar in the case of routes A and C, the total processing time was practically the same for both the routes ($\sim$ 11 h). Considering the actual T_{IH} for bainite transformation to be 300 °C in the case of routes A and C, it could be discerned from the experiments that in the course of route B, most of the bainite actually formed at temperatures well above the T_{IH} (300 °C) that was reached relatively slowly during air cooling (average cooling rate 0.5 °C s^{-1}).

4.2 Microstructures

Both the steels S1 and S2 displayed the highest fractions of BF after processing via route A (S1-A: 74, and S2-A: 77%), intermediate fractions after route C (S1-C: 67 S2-C: 60%), and the lowest fractions after route B (S1-B: 59 and S2-B: 52%).

dimensions may not be heated and/or cooled at rates as fast as small specimens used in physical simulation, especially without induction heating capability, for instance. As far as the amenability to industrial processing is concerned, route A was the most appropriate approach to emulate the physical simu-

On the other hand, martensite fractions were at the same level for steel S1 following routes A and C (S1-A: 9, S1-C: 10%), whereas for steel S2 the corresponding fraction was slightly higher than steel A when processed via route C (S2-C: 12%), but significantly lower following route A (S2-A: 5%) because of better stabilization of RA. Referring to Fig. 3, both the steels S1 and S2 had very similar microstructural characteristics, though the most obvious difference was noticeable in the case of route C. Whereas relatively higher carbon content (0.48 wt.%) in steel S2 enabled stabilization of more austenite at RT (28 RA%), steel S1 with marginally lower carbon content (0.4 wt.%) displayed formation of higher bainite fraction with more film-like morphology of RA (23 RA%). In general, the C_{RA} did not vary remarkably, and the main trend suggested the lowest C_{RA} in the samples processed through route B. C_{RA} is often assumed to depend on the fraction of bainite formed, as BF, regardless of its tetragonality, tends to transfer most of its carbon into the adjacent austenite during the course of bainite transformation. However, this assumption seemed true only for samples of steel S1, whereas in the case of steel S2, C_{RA} was higher in the S2-C sample than in the S2-A sample despite the lower BF fraction in the S2-C sample compared to the S2-A sample. This observation can be rationalized by considering the morphology of RA, which is less stable in the form of large, blocky M/A grains compared to fine film-like constituents (Ref 9, 11). Processing via routes A and C resulted in more than 10% of fine film-like RA constituents in both steels (S1-A: 15, S1-C: 16, S2-A:15, and S2-C: 11%), whereas in the case of route B only a small fraction of RA was film-like (S1-B: 3, S2-B: 1%), as illustrated in Fig. 5. However, by comparing S2-A and S2-C samples, it was found that C_{RA} was higher in the S2-C sample, which would indicate higher stability of RA in the S2-C sample, though more BF and more film-like RA were obtained in the S2-A sample. Surprisingly, however, tensile property evaluation revealed higher ductility for the S2-A sample compared to that of the S2-C sample (see Table 4) and requires further investigation.

The morphology of BF in S1-B and S2-B samples was mostly coarser compared to those seen in S1-C and S2-C samples, presumably because T_{IH} was not the same (Route B: 350 °C, Route C: 300 °C). It is presumed that coalescence of coarse upper BF plates occurred during isothermal holding in route B resulting in coarse BF. In both steels S1 and S2, the differences in microstructures of samples following routes B and C prior to reaching the T_{IH} could be corroborated with the microstructures of corresponding samples from physical simulation experiments. In spite of the planned isothermal holding at 350 °C, the samples of route B actually resembled the microstructures of Gleeble samples S1-375 and S2-375 obviously due to slow cooling, whereas samples following route C had similar characteristic features as those of S1-350 and S2-350 samples. In other words, the results of physical simulation experiments indicate that in the case of route B, BF had formed at temperatures close to 375 °C or even higher, whereas in the case of route C, the finest plates of bainite observed in the microstructure might have formed at 300 °C, with the possibility of at least a fraction transforming at somewhat higher temperatures up to 350 °C.

Also, because there was no ausforming in the case of route C, the time required to reach the T_{IH} was shorter and it is possible that the incubation of bainite formation was hindered, too. Thus, the probability of austenite transforming to bainite in the samples of route C before reaching the desired T_{IH} was

relatively low. This was considered beneficial in respect of avoiding the formation of undesired coarse upper bainite. In comparison with route A, the bainite transformation kinetics must have been somewhat slower in route C, thereby leading to a relatively lower fraction of fine bainite formed, and a higher fraction of austenite retained for both the steels (S1-A: 17, S1-C: 23% and S2-A: 18, S2-C: 28%). More importantly, the fraction of blocky RA, however, increased in both steels, especially in steel S2 (route A: 3%, route C: 17%). Thus, the difference in the morphology of RA achieved via the three processing routes in the current study was mainly controlled by the T_{IH}, as even a small temperature difference of 25 °C affected the morphology of the transformed bainite (Ref 7). Despite the variation in cooling paths and bainite transformation behavior, the findings of this study are in sharp contrast with the conclusions of Hu et al. (Ref 6), who suggested retardation of bainite formation kinetics following ausforming at a temperature above 400 °C. Hence, the reduction in ausforming temperature down to 400 °C or below could be an appropriate target for future studies, though either the amount of strain applied should be reduced or the chemical composition should be adjusted in order to include increased amounts of austenite stabilizing elements to decrease M_s and, moreover, to prevent the strain and/or stress-induced phase transformations (Ref 7, 14, 15).

The ECDs (Fig. 4c and d) measured on S2-A and S2-B samples can be considered to be of the practically same level (S2-A: 2.0 vs. S2-B: 2.5 μm). In the case of route A, the presence of refined BF increased the fraction of small ECDs, whereas in the case of S2-B sample, a relatively high fraction of fine, fresh martensite formed from the carbon-enriched austenite during final cooling, resulting in decreased mean ECD. However, it should be emphasized that the fraction of large grains observed in the S2-B sample was slightly greater than that of the S2-A sample, obviously due to the significant formation of coarse granular and/or coalesced bainite in the S2-B sample.

4.3 Mechanical Properties

Higher RA content (see Table 3) achieved via route B compared to route A correlated quite linearly with hardness values, despite high fractions of martensite in S1-B and S2-B samples. Because of the multiphase structures resulting from the two processing routes comprising different phase fractions, there was only little direct evidence of a correlation between the morphology and the fineness of BF and mechanical properties. Although the martensite fractions in S1-A and S2-A (9 and 5%, respectively) samples were lower than those of S1-C and S2-C (10% and 12%, respectively) samples, the S1-A and S2-A samples exhibited higher hardness values and yield strengths in comparison with S1-C and S2-C samples (Table 4). Even though S1-C and S2-C samples revealed relatively lower yield strengths and hardness values, they possessed comparatively good ductility (A_t: 17 and 10% for S1-C and S2-C, respectively). In route B, fresh martensite present in M/A constituents contributed more to the strength and therefore, S2-B did exhibit inadequate elongation (see Fig. 5), despite the presence of relatively high fractions of RA (23%, of which 22% was blocky-type) and coarse upper bainite in the steel. However, in S1-B sample, the lack of fine film-like RA (estimated about 3%) did not cause a significant loss of ductility, when compared with S1-A and S1-C samples (S1-A: 12.8%, S1-B: 14.9%, S1-

C: 17.0%), though blocky RA was expected to have lower stability. Instead, S1-B sample was even more ductile than S1-A sample that contained an appreciably higher fraction of film-like RA (S1-A: 15% and S1-B: 3%), though the total fraction of RA was higher in S1-B sample (21%) than in S1-A sample (17%).

In effect, the most prominent combination of strength and ductility could be reached with a mixed multiphase microstructure observed in S1-C and S2-A samples. Zhang et al. (Ref 10) proposed that ausforming above B_s had only a negligible effect on the bainite morphology and this was at least applicable in the case of steel S1, though steel S2 with a slightly higher carbon content showed the expected potential of ausforming. This, however, needs further clarification using in situ measurements planned in the next phase of the study. All the same, very fine bainitic microstructures and promising mechanical properties could be achieved from the entire processing window (from slow cooling and high T_{IH} to fast cooling and low T_{IH}). Further work, however, is needed to exploit and optimize fully the potential of the increased strength of austenite following low-temperature ausforming in achieving the ultrafine bainitic plates as well as improved property combinations in medium-carbon steels.

5. Conclusions

Different processing routes were conducted in order to evaluate and design a suitable low-temperature processing route (with and without ausforming) for the development of ultrafine bainite in some medium-carbon steels. The results suggest that the refinement of bainite to an ultrafine level could be reached by fast cooling (20 C·s^{-1}) down to a low T_{IH} (300 °C, route A), while the expected advantages of the fineness of the bainitic structure on the mechanical properties were obtained only in one of the two studied medium-carbon steels. In the case of 0.4 wt.% C-steel, the real benefit of producing very fine bainite by the complex cooling and ausforming process could not be explained in terms of measured mechanical properties, while in the case of 0.48C-steel the processing route leading to the finest bainitic structure, i.e., route A, resulted in the best combination of hardness, strength, and ductility. The following conclusions can be drawn:

- Lower bainite formation temperature in the route A not only refined the bainite in terms of plate size compared to the route B but also led to an increased fraction of bainite and decreased fraction of RA (S1-A: 17 vs. S1-B: 21%, S2-A: 18 vs. S2-B: 23%) and martensite, as expected.
- Equivalent circle diameters measured on the S2-A and S2-B samples did not vary remarkably from each other, although the appearance of the two microstructures was visibly different. The ECD originated from refined bainite (BF and film-like RA) in the S2-A sample and a mixture of coarse bainite and high-carbon martensite in the S2-B sample.
- Microstructure-property relationships in studied steels raised interesting observations, as multiphase bainite-martensite-austenite microstructure was found to be more beneficial for improved mechanical property combination, compared to very fine bainitic-austenitic microstructure.

- Isothermal holding without prior ausforming (route C) also resulted in quite similar mixed microstructures, and the mechanical properties did not deviate significantly from other routes following ausforming (routes A and B), except for slightly lower hardness values and ultimate tensile strengths. A reduction in hardness in non-ausformed samples (route C) originated from relatively less martensite content, whereas a high RA fraction compensated the properties by imparting improved ductility, in comparison with samples of other routes following ausforming. S2-C sample (0.48 wt.% C) showed more RA at RT, but despite being essentially of blocky morphology, the average carbon enrichment (1.18%) was significant. On the other hand, the S1-C sample (0.4 wt.% C) exhibited somewhat lower C_{RA} (0.97%), though a significant fraction of ultrafine bainite was realized in the sample along with largely film-like RA.
- Despite the presence of high RA, 0.48 wt.% C-steel S2 exhibited higher strength and hardness and lower ductility in all three samples processed via routes A-C in comparison to steel 0.4 wt.% C-steel S1. That could be explained in respect of the size and morphology of the microstructural features, viz. the BF as well as RA.

Data Availability

The raw/processed data required to reproduce these findings cannot be shared at this time, as the data also form part of an ongoing study.

References

1. F.G. Caballero, H.K.D.H. Bhadeshia, K.J.A. Mawella, D.G. Jones, and P. Brown, Very Strong Low Temperature Bainite, *Mater. Sci. Technol.*, 2002, **18**, p 279–284. https://doi.org/10.1179/026708301225000725

2. F.G. Caballero and H.K.D.H. Bhadeshia, Very Strong Bainite, *Curr. Opin. Solid State Mater. Sci.*, 2004, **8**, p 251–257. https://doi.org/10.1016/j.cossms.2004.09.005

3. C. Garcia-Mateo and F.G. Caballero, Ultra-High-Strength Bainitic Steels, *ISIJ Int.*, 2005, **45**, p 1736–1740. https://doi.org/10.2355/isijinternational.45.1736

4. W. Gong, Y. Tomota, Y. Adachi, A.M. Paradowska, J.F. Kelleher, and S.Y. Zhang, Effects of Ausforming Temperature on Bainite Transformation, Microstructure and Variant Selection in Nanobainite Steel, *Acta Mater.*, 2013, **61**, p 4142–4154. https://doi.org/10.1016/j.actamat.2013.03.041

5. A. Navarro-López, J. Hidalgo, J. Sietsma, and M.J. Santofimia, Unravelling the Mechanical Behaviour of Advanced Multiphase Steels Isothermally Obtained Below M_s, *Mater. Des.*, 2020, **188**, p 108484. https://doi.org/10.1016/j.matdes.2020.108484

6. H. Hu, G. Xu, F. Dai, J. Tian, and G. Chen, Critical Ausforming Temperature to Promote Isothermal Bainitic Transformation in Prior-Deformed Austenite, *Mater. Sci. Technol. UK*, 2019, **35**, p 420–428. https://doi.org/10.1080/02670836.2019.1567663

7. P.M. Kaikkonen, M.C. Somani, I.H. Miettunen, D.A. Porter, S.T. Pallaspuro, and J.I. Kömi, Constitutive Flow Behaviour of Austenite at Low Temperatures and Its Influence on Bainite Transformation Characteristics of Ausformed Medium-Carbon Steel, *Mater. Sci. Eng. A.*, 2020, **775**, p 9–11. https://doi.org/10.1016/j.msea.2020.138980

8. M. Zorgani, C. Garcia-Mateo, and M. Jahazi, Effects of Ausforming Temperature on Carbide-Free Bainite Transformation and Its Correlation to the Transformation Plasticity Strain in a Medium C- Si-Rich Steel, *Mater. Charact.*, 2021 https://doi.org/10.1016/j.matchar.2021.111124

9. C. Garcia-Mateo and F.G. Caballero, The Role of Retained Austenite on Tensile Properties of Steels With Bainitic Microstructures, *Mater. Trans.*, 2005, **46**, p 1839–1846. https://doi.org/10.2320/matertrans.46.1839

10. M. Zhang, Y.H. Wang, C.L. Zheng, F.C. Zhang, and T.S. Wang, Effects of Ausforming on Isothermal Bainite Transformation Behaviour and Microstructural Refinement in Medium-Carbon Si-Al-Rich Alloy Steel, *Mater. Des.*, 2014, **62**, p 168–174. https://doi.org/10.1016/j.matdes.2014.05.024

11. M. Zorgani, C. Garcia-Mateo, and M. Jahazi, The Role of Ausforming in the Stability of Retained Austenite in a Medium-C Carbide-Free Bainitic Steel, *J. Mater. Res. Technol.*, 2020, **9**, p 7762–7776. https://doi.org/10.1016/j.jmrt.2020.05.062

12. J. Li, F. Liu, S. Wang, J. Li, Y. Liu, and Q. Meng, Effect of Two-Step Bainite Treatment on the Morphology and Texture of Retained Austenite and Mechanical Properties of Austenitizing Pretreated Transformation-Induced Plasticity Steel, *Mater. Sci. Eng. A.*, 2020, **771**, p 138567. https://doi.org/10.1016/j.msea.2019.138567

13. A. Eres-Castellanos, L. Morales-Rivas, A. Latz, F.G. Caballero, and C. Garcia-Mateo, Effect of Ausforming on the Anisotropy of Low Temperature Bainitic Transformation, *Mater. Charact.*, 2018, **145**, p 371–380. https://doi.org/10.1016/J.MATCHAR.2018.08.062

14. A. Eres-Castellanos, J. Hidalgo, M. Zorgani, M. Jahazi, I. Toda-Caraballo, F.G. Caballero, and C. Garcia-Mateo, Assessing the Scale Contributing Factors of Three Carbide-Free Bainitic Steels: a Complementary Theoretical and Experimental Approach, *Mater. Des.*, 2021, **197**, p 109217. https://doi.org/10.1016/j.matdes.2020.109217

15. A. Eres-castellanos and F.G. Caballero, Stress or Strain Induced Martensitic and Bainitic Transformations during Ausforming Processes, *Acta Mater.*, 2020 https://doi.org/10.1016/j.actamat.2020.03.002

16. S.M.C. van Bohemen, Bainite Growth Retardation Due to Mechanical Stabilisation of Austenite, *Materialia.*, 2019, **7**, p 100384. https://doi.org/10.1016/j.mtla.2019.100384

17. B. Avishan, S. Golchin, and S. Yazdani, Elongation Improvement in Nano Bainite Steel Obtained from Plastically Deformed Primary Austenite, *Philos. Mag.*, 2020, **100**, p 2244–2261. https://doi.org/10.1080/14786435.2020.1764654

18. S.M.C. Van Bohemen, Bainite, and Martensite Start Temperature Calculated with Exponential Carbon Dependence, *Mater. Sci. Technol.*, 2012, **28**, p 487–495. https://doi.org/10.1179/1743284711Y.0000000097

19. J. Miettinen, S. Louhenkilpi, H. Kytönen, and J. Laine, IDS: Thermodynamic-Kinetic-Empirical Tool for Modelling of Solidification, Microstructure and Material Properties, *Math. Comput. Simul.*, 2010, **80**, p 1536–1550. https://doi.org/10.1016/j.matcom.2009.11.002

20. A. Kumar and A. Singh, Mechanical Properties of Nanostructured Bainitic Steels, *Materialia.*, 2021, **15**, p 101034. https://doi.org/10.1016/j.mtla.2021.101034

21. C. Garcia-Mateo, A. Eres-Castellanos, F. García Caballero, P. Kaikkonen, A. Latz, A. Pohjonen, D.A. Porter, A. Ray, L. Bracke, S. Schreiber, M. Somani, Towards industrial applicability of (medium C) nanostructured bainitic steels (TIANOBAIN-RFCS-709607), 2020. doi: http://dx.doi.org/https://doi.org/10.20350/digitalCSIC/12589

22. N. Saunders, Z. Guo, P. Miodownik, and J.-P. Schillé, (2004) The Calculation of TTT and CCT Diagrams for General Steels, JMatPro Softw. Lit. 1–12. 10.1.1.565.9926

23. ASTM E 562–01, Standard Test Method for Determining Volume Fraction by Systematic Manual Point Count, ASTM Int. (2000). https://doi.org/10.1520/E0562-01

24. S.W. Ooi, Y.R. Cho, J. K. Oh, H.K.D.H. Bhadeshia, Carbon Enrichment in Residual Austenite During Martensitic Transformation, In: Proc. Int. Conf. Martensitic Transform. ICOMAT-08, 2009 179–185

25. ASTM E8, ASTM E8/E8M Standard Test Methods for Tension Testing of Metallic Materials 1, Annu. B. ASTM Stand. 4. (2010) 1–27. doi:https://doi.org/10.1520/E0008

26. A. Pohjonen, P. Kaikkonen, O. Seppälä, J. Ilmola, V. Javaheri, T. Manninen, and M. Somani, Numerical and Experimental Study on Thermo-Mechanical Processing of Medium-Carbon Steels at Low Temperatures for Achieving Ultrafine-Structured Bainite, *Materialia.*, 2021, **18**, p 101150. https://doi.org/10.1016/j.mtla.2021.101150